Study of the $\gamma\gamma$ decays of the $\chi_{c2}(1^3P_2)$ and $\chi_{c0}(1^3P_0)$ charmonium resonances

M. Ambrogiani,[2] S. Argirò,[6] S. Bagnasco,[6] W. Baldini,[2] D. Bettoni,[2] G. Borreani,[6] A. Buzzo,[3] R. Calabrese,[2] A. Ceccucci,[6] R. Cester,[6] P. Dalpiaz,[2] X. Fan,[5] G. Garzoglio,[1] K. E. Gollwitzer,[4] A. Hahn,[1] S. Jin,[5] J. Kasper,[5] G. Lasio,[4] M. Lo Vetere,[3] E. Luppi,[2] P. Maas,[5] M. Macrì,[3] M. Mandelkern,[4] F. Marchetto,[6] M. Marinelli,[3] W. Marsh,[1] M. Martini,[2] E. Menichetti,[6] R. Mussa,[2] M. M. Obertino,[6] M. Pallavicini,[3] N. Pastrone,[6] C. Patrignani,[3] T. K. Pedlar,[5] J. Peoples, Jr.,[1] S. Pordes,[1] E. Robutti,[3] B. Roccuzzo,[6] J. Rosen,[5] P. Rumerio,[6] A. Santroni,[3] M. Savrié,[2] J. Schultz,[4] K. K. Seth,[5] G. Stancari,[2] M. Stancari,[4] J. Streets,[1] A. Tomaradze,[5] S. Werkema,[1] and G. Zioulas[4]

(Fermilab E835 Collaboration)

[1]*Fermi National Accelerator Laboratory, Batavia, Illinois 60510*
[2]*Istituto Nazionale di Fisica Nucleare and University of Ferrara, I-44100 Ferrara, Italy*
[3]*Istituto Nazionale di Fisica Nucleare and University of Genova, I-16146 Genova, Italy*
[4]*University of California at Irvine, Irvine, California 92697*
[5]*Northwestern University, Evanston, Illinois 60208*
[6]*Istituto Nazionale di Fisica Nucleare and University of Torino, I-10125, Torino, Italy*

(Received 12 April 2000; published 2 August 2000)

We report the branching ratios of the $\chi_{c2}(1^3P_2)$ and $\chi_{c0}(1^3P_0)$ charmonium resonances to two photons using event samples collected by Fermilab experiment E835 in the reactions $\bar{p}p \to \chi_{c2}(1^3P_2)[\chi_{c0}(1^3P_0)]$. Our result for the χ_{c2} is $B(\chi_{c2} \to \gamma\gamma) = (1.35 \pm 0.25 \pm 0.12) \times 10^{-4}$. We set a 95% upper limit for the χ_{c0} branching ratio $B(\chi_{c0} \to \gamma\gamma)$ at 2.09×10^{-4}.

PACS number(s): 14.40.Gx, 13.40.Hq, 13.75.Cs

I. INTRODUCTION

One of the first applications of perturbative QCD (PQCD) [1] was the analysis of the electromagnetic decays of heavy quark-antiquark systems, where the annihilation of the heavy quark and antiquark was assumed to be a short-distance process that, because of asymptotic freedom, can be computed in perturbation theory. Recent work in PQCD has focused on these processes because of their relative simplicity and because they are among the few phenomena for which useful predictions can be made [2–6]. The study of these decays provides an important test of QCD as well as a means for estimation of the strong coupling constant α_s.

We report measurements of the $\gamma\gamma$ decays of the χ_{c2} and χ_{c0} charmonium resonances formed in $\bar{p}p$ annihilations. Within the framework of PQCD [7], the ratio of the partial widths $\Gamma(\chi \to \gamma\gamma)/\Gamma(\chi \to gg)$ is determined only by α_s, evaluated at the charm quark mass.

II. EXPERIMENTAL METHOD

A. Technique

Fermilab experiment E835 is devoted to the study of charmonium spectroscopy by direct formation of $c\bar{c}$ states in $\bar{p}p$ annihilation at the Fermilab Antiproton Accumulator ring [8]. A cylindrical jet of clusterized hydrogen molecules (7 mm diameter, $\rho_{max} \sim 3.0 \times 10^{14}$ atoms/cm^3) [9] intersects a beam of up to 80 mA of antiprotons ($\sim 8 \times 10^{11}$ stored particles) circulating in the Accumulator to produce instantaneous luminosities of up to 5×10^{31} cm^{-2} s^{-1}. The jet density is increased to keep the instantaneous luminosity constant as the circulating antiproton current decreases.

The antiproton beam is stochastically cooled such that the rms spread in the center-of-mass energy, $\sqrt{s}$, is ~ 0.4 MeV; the uncertainty in the mean center-of-mass energy for these data is estimated to be ~ 0.2 MeV. The $c\bar{c}$ resonance parameters are determined precisely by measuring the excitation curve obtained by stepping the energy of the antiproton beam across the resonance. Advantages of this technique are that all $c\bar{c}$ states can be produced directly in $\bar{p}p$ annihilations and that the precision of the mass and width determination of these states does not depend on the resolution of the detector system but is determined only by event statistics and the knowledge of the antiproton beam energy and energy spread.

For this analysis, we examined two methods for determining the $\gamma\gamma$ branching ratios of the χ_{c2} and χ_{c0}. The first is the usual method of fitting the data to the sum of background and Breit-Wigner resonance signals and determining the cross sections for the $\gamma\gamma$ reactions. The second, which we report here, is the use of ratios of the rates to the final states: $\gamma\gamma$ and $J/\psi\gamma$. This method takes advantage of the fact that the χ branching ratios to $J/\psi\gamma$ are relatively well measured and do not significantly contribute to the error in the $\gamma\gamma$ branching ratios. In addition, systematic errors due to uncertainties in the beam momentum and luminosity do not appear in a determination using ratios of rates measured simultaneously. This feature is particularly valuable for the E835 running where the beam momentum was uncertain for part of the data due to failures of elements of the beam position monitoring system of the Antiproton Source. The momentum uncertainty is especially relevant for the narrow ($\Gamma = 2$ MeV) χ_{c2} state.

B. Detector

We select electromagnetic final states as tags of charmonium formation. This makes it possible to extract a clean signal despite the large hadronic background. The detector,

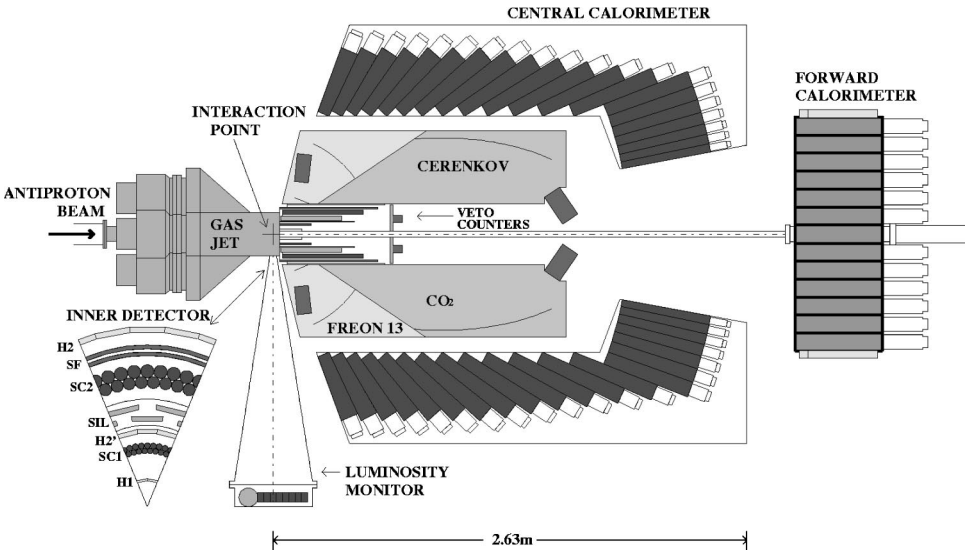

FIG. 1. The E835 detector.

shown in Fig. 1, is therefore optimized for the detection and identification of photons and electrons. It has full coverage in azimuthal angle (ϕ), and consists of a cylindrical central detector and a planar forward system. The central detector contains 3 azimuthally segmented scintillator hodoscopes identified as H1, H2′, H2, two sets of straw tubes [10] for tracking in azimuth, a scintillating-fiber tracker [11] for tracking in θ, a 16 cell threshold gas Čerenkov counter [12] for electron identification and a 1280 element [20 rings (θ), each comprised of 64 counters (ϕ)] lead-glass calorimeter (CCAL) [13] for measuring the directions and energies of photons and electrons. CCAL covers polar angles $11° < \theta < 70°$. The forward electromagnetic calorimeter of 144 elements is not used in this analysis. All counters are equipped with both time and pulse-height readout. The time measurements allow the rejection of signals from out-of-time events while the pulse-height measurements on the scintillation hodoscopes and Čerenkov counters allow rejection of photon conversions and Dalitz pairs. For this analysis, the relevant element of the forward system is FCV, a segmented plastic scintillating hodoscope covering from 2 ° to 10 ° in θ, which identifies charged particles and serves as a veto in the neutral trigger. A luminosity monitor [14] provides an absolute luminosity measurement with a statistical precision of better than 0.1% and an estimated systematic error of $\pm 2.5\%$, by measuring $\bar{p}p$ forward elastic scattering through the detection of proton recoils at $\theta = 86.5°$ in three solid state detectors.

C. Trigger

The total $\bar{p}p$ cross section is as large as 70 mb in the energy region of interest, corresponding to an interaction rate of up to ~ 3 MHz at the experiment peak luminosity of $\sim 5 \times 10^{31}$ cm^{-2} s^{-1}.

Events of interest are selected by a fast hardware trigger (level 1), which reduces the rate to <2.5 kHz, and then transferred to a set of processors where a software filter (level 2) is applied before recording the events on tape [15]. The level-1 trigger accepts in parallel: final states containing either an electron and positron ($a1$) or two photons ($a2$) of large invariant mass; all neutral final states where $\geqslant 80\%$ of the initial state energy is contained in the central calorimeter (b). A random gate trigger is generated with a pulser operating between 1 Hz and 10 Hz to obtain data used to study pileup and dead time.

The element common to the $a1$ and $a2$ triggers is an algorithm applied to central calorimeter signals that is tailored to accept e^+e^- and $\gamma\gamma$ final states with full efficiency [16]. The trigger requires the presence of two energy deposits, each with energy above a θ-dependent threshold and approximately coplanar with the $\bar{p}$ direction. It is implemented as follows. To reduce the number of signals to a manageable level, the analog signals from the individual counters are summed to produce a matrix of 40 supermodules (8 in. ϕ by 5 in. θ), with appropriate overlap to ensure that 95% of the energy from an individual γ or electron is contained within one supermodule. The reduction is performed in two successive stages, from 1280 to 160 signals, and then from 160 to 40. In the first, signals from groups of 9 adjacent counters (same θ) are added to form 8 octants, with one counter overlap, for each of the 20 θ values. In the second, the resulting 160 signals (8 in. ϕ by 20 in. θ) are combined into sums over θ in groups of 5, weighted so that the trigger efficiency is independent of θ, again allowing a one counter overlap. The 40 analog signals from the supermodules are integrated and discriminated. The thresholds are set to $\sim 60\%$ of the energies for a two-body reaction. This loose requirement permits triggering on decays to inclusive channels containing J/ψ or η_c. The discriminator outputs from the 5 supermodules in each octant are logically ORed to form the 8 logic signals used for triggering.

For the $e^+e^-X(a1)$ final state, we require that two of these signals come from opposing octants (1 against 3) to impose approximate coplanarity ($PBG3$). The trigger rate is further reduced by requiring a coincidence between corresponding (consistent ϕ) elements of the H1 and H2 hodoscopes and of the Čerenkov counter.

To select $\gamma\gamma$ ($a2$) events, we require that two of the CCAL logic signals come from opposing octants [1 against

TABLE I. Summary of data for the χ_{c2} resonance. The $\gamma\gamma$ events satisfy the $\alpha=0.45$ acceptance cut and those marked by an asterisk are used for the ratio determination.

$\sqrt{s}$ (MeV)	$\mathcal{L}$ (nb^{-1})	$N_{\gamma\gamma}$	$N_{J/\psi\gamma}$	$\epsilon_{\gamma\gamma}$
3526.0	44319	779		0.75
3529.1	2328	40		0.77
3535.5	1304	20		0.75
3544.8	998	12	8	0.81
3554.7	490	9	122	0.76
3555.2*	519	13	234	0.79
3555.6*	411	12	205	0.76
3555.9*	516	16	315	0.74
3556.0*	994	34	593	0.74
3556.1*	778	26	453	0.83
3556.1*	413	10	271	0.75
3556.2*	521	14	354	0.78
3556.3*	501	13	302	0.75
3556.3*	752	18	500	0.73
3556.7*	810	28	436	0.73
3556.8*	401	11	154	0.76
3557.3*	896	18	354	0.79
3557.9	383	11	52	0.75
3576.0	1606	270		0.75
3629.0	26823		59	
3686.2	8012	97		0.63

TABLE II. Summary of data for the χ_{c0} resonance. The $\gamma\gamma$ events satisfy the $\alpha=0.40$ acceptance cut and those marked by an asterisk are used for the ratio determination. The bottom two rows give the recorded and feeddown event totals for data points at the h_c and ψ', used to check the feeddown calculation for the $\alpha=0.45$ acceptance cut.

$\sqrt{s}$ (MeV)	$\mathcal{L}$ (nb^{-1})	$N_{\gamma\gamma}$	$N_{J/\psi\gamma}$	N_{feed}	$\epsilon_{\gamma\gamma}$
3215.7	420	25	0	17.0 ± 1.5	0.77
3269.4	412	15	1	14.5 ± 1.3	0.83
3318.8	951	23	0	22.9 ± 1.9	0.77
3406.8*	926	23	15	17.3 ± 1.6	0.78
3414.8*	585	14	12	9.1 ± 1.1	0.74
3414.8*	353	9	6	6.6 ± 0.8	0.81
3418.1*	146	5	7	3.0 ± 0.5	0.81
3418.5*	692	9	22	8.5 ± 1.0	0.78
3429.5*	349	7	3	6.2 ± 0.7	0.82
3429.9*	390	7	3	5.5 ± 0.8	0.83
3494.4	503	7	2	6.6 ± 0.8	0.77
3510.6	6459	88			0.76
3526.0	44319	630			0.75
3529.1	2328	34			0.77
3535.5	1304	15			0.75
3629.0	26823		59		
3525.8	3934	63		61.2 ± 4.3	0.77
3686.1	996	7		6.3 ± 0.9	0.60

1, a stricter coplanarity condition ($PBG1$)]. We demand that no charged particles be detected in the final state, implemented by requiring the charged veto, which is on if there is at least one signal in the FCV or at least one hit above threshold in both a H1 element and one of the three corresponding H2′ elements, to be off. These counter systems together fully cover the polar angle range $2°\leqslant\theta\leqslant65°$ over the complete azimuth.

To select all-neutral (b) events, we sum the pulse heights from the entire central calorimeter, excluding the two rings with the smallest θ's, for an angular acceptance of $13°\leqslant\theta\leqslant70°$. The total energy condition ($ETOT$) is met if the sum pulse exceeds a threshold corresponding to 80% of the initial state energy. For b, we require that the charged veto be off.

In this analysis, a cluster consists of a 3×3 grid of counters containing >20 MeV centered on a block containing >5 MeV. Clusters are found by the software trigger, where we convert the CCAL pulse heights to energies, determine cluster coordinates and energies, and calculate the invariant masses of all pairs of clusters. The clustering algorithm used on line is a simplified version of the one used in the off-line analysis [17]. All events, for which any two CCAL clusters have invariant mass $\geqslant2.2$ GeV, are recorded and constitute the data set for this analysis.

D. Data collection

Experiment E835 took data between October 1996 and September 1997. Data were taken in the vicinity of the χ_{c2} and χ_{c0} as well as at the η_c, J/ψ, ψ', $h_c(\sim3526$ MeV) and in the interval 3580 MeV$\leqslant\sqrt{s}\leqslant$3660 MeV ($\eta_c'$ search). The data used for this analysis are summarized in Tables I and II. The integrated luminosity for the χ_{c2} scan (3554.7 MeV$\leqslant\sqrt{s}\leqslant$3557.9 MeV) is 8.38 pb^{-1} and that for the χ_{c0} scan (3406.8 MeV$\leqslant\sqrt{s}\leqslant$3429.9 MeV) is 3.44 pb^{-1}. The remaining data in the tables are used for background determination.

III. DATA ANALYSIS

A. Cluster timing

The most important element of the upgrade from E760 to E835 is the addition of pulse shaping to the Central Calorimeter signals and time-to-digital converters (TDCs) to nearly every detector in the apparatus. This upgrade was motivated by the significantly greater instantaneous luminosity available to E835 and is particularly important for low signal, high background channels such as $\gamma\gamma$, where accidental coincidences due to pion production lead to background events as well as trigger and analysis inefficiencies. For CCAL, TDC information is present with nearly unit efficiency for clusters with energies >75 MeV. The efficiency falls to ~0.5 at 30 MeV and to zero at ~20 MeV. The data for all of the counters in a cluster are corrected for slewing and referred to a time derived from the analog signals from the first stage of summing of CCAL. For each cluster we consider the counters with the two largest numbers of analog-to-digital converter (ADC) counts. If neither has TDC informa-

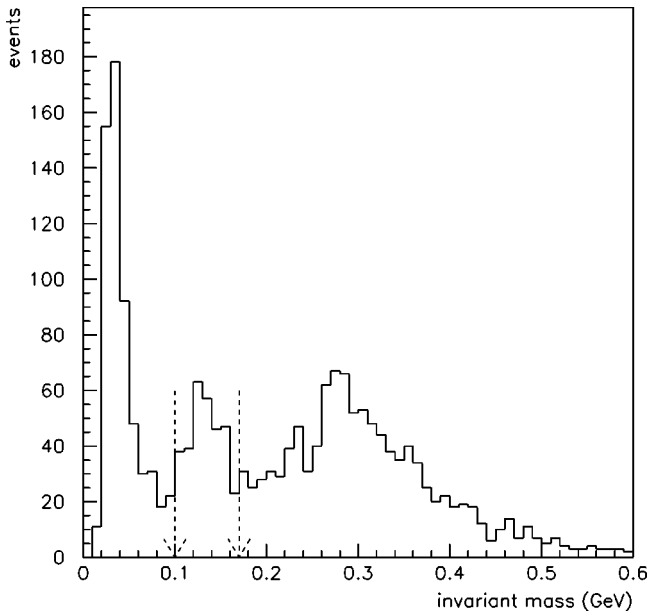

FIG. 2. The invariant mass distribution of undetermined extra clusters paired with candidate photons for events satisfying the kinematical fit to $\gamma\gamma$. Events where the invariant mass of any pair is within 35 MeV of the π^0 mass, as indicated by the dashed lines, are rejected. No η peak is seen.

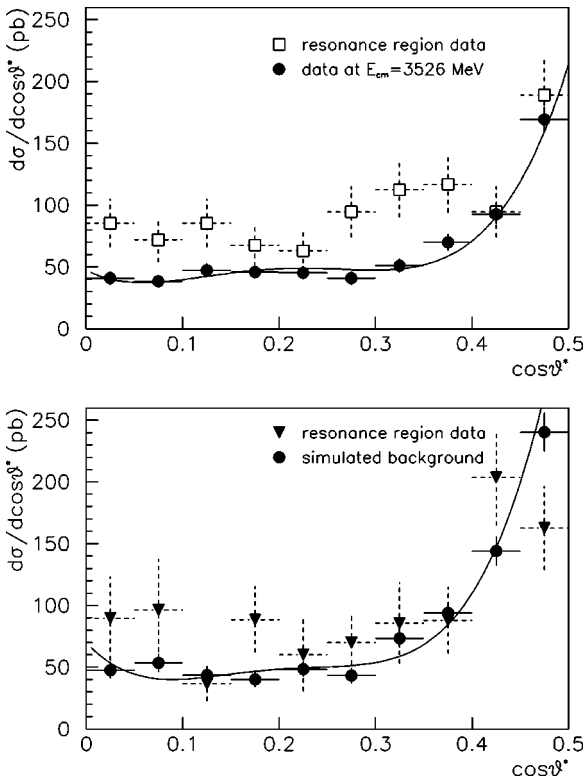

FIG. 3. Differential cross sections derived from the on-resonance and background data for the χ_{c2} and χ_{c0} resonances. The upper plot shows $\gamma\gamma$ candidates at 3555.2 MeV$\leqslant\sqrt{s}\leqslant$3557.3 MeV along with the background corresponding to $\gamma\gamma$ candidates at approximately 3526 MeV. The lower plot shows $\gamma\gamma$ candidates at 3406.8 MeV$\leqslant\sqrt{s}\leqslant$3429.9 MeV along with the background for the same energies derived from simulated events obtained using the feeddown calculation described in the text. The curves are polynomial fits to the background cross sections.

tion, the cluster is identified as *undetermined*. If either has a corrected time within 10 ns of the reference time, the cluster is identified as *in time*. The cluster is otherwise identified as *out of time*.

B. $\gamma\gamma$ event selection

Event selection is optimized to select $\gamma\gamma$ candidates with high efficiency while reducing the background from $\pi^0\pi^0$ and $\pi^0\gamma$ final states to an acceptable level. These candidate events satisfy the $a2$ and/or b trigger with the largest two-cluster invariant mass $\geqslant$2.7 GeV. We require this invariant mass to be within 20% of $\sqrt{s}$ and the corresponding CCAL clusters to satisfy $15°<\theta<60°$.

A more stringent acceptance limitation is imposed subsequently. A 4 constraint kinematical fit to the $\gamma\gamma$ hypothesis is performed using the SQUAW program [18], and the events with a nominal confidence level below 5% are discarded.

While events containing symmetrically decaying π^0's are readily distinguished from $\gamma\gamma$ events [17], a small fraction of the abundant $\pi^0\gamma$ and $\pi^0\pi^0$ events satisfy the selection when the π^0('s) decays highly asymmetrically. Further cuts are imposed to reduce this background. No in-time extra clusters are allowed in the candidate events, and out-of-time extra clusters are disregarded. Figure 2 gives the invariant mass distribution for undetermined extra clusters paired with candidate photons and shows a clear π^0 peak. We reject an event if the invariant mass of any pair falls within 35 MeV of the π^0 mass (135 MeV). We observe no evidence for contamination by η inclusive events.

For a category of $\pi^0\gamma$ and $\pi^0\pi^0$ events, the low energy γ('s) escapes detection because it is below the energy threshold or is not contained in the angular acceptance of CCAL. This background is suppressed by exploiting the difference between the angular distribution of the signal and that of the background. The $\pi^0\pi^0$ and $\pi^0\gamma$ angular distributions are strongly peaked in the forward direction leading to a forward-peaked $\gamma\gamma$ background distribution as shown in Fig. 3. Hence, an acceptance cut is chosen, $\cos\theta^*<\alpha$, where θ^* is the center-of-mass angle, to maximize the significance of the signal. We determine α *a priori*, as described in the Appendix, maximizing the power for discrimination between the nonresonant and resonant hypotheses. We find that α is larger at the χ_{c2} ($\alpha=0.45$) than at the χ_{c0} ($\alpha=0.40$) since the signal to background is greater and the background rises less abruptly with $\cos\theta^*$ in the former case. The geometrical acceptance of the detector for the $\gamma\gamma$ channel is unity for $\cos\theta^*\leqslant 0.6$.

Because of inefficiency in the charged veto, a small fraction of the e^+e^- events is selected by the $a2$ trigger. This contamination is only important at the ψ', used as a background point in this analysis, but the following selection is applied to all of the data for consistency. To eliminate these events, we impose a selection criterion when there are hodoscope or Cerenkov signals associated with both selected CCAL clusters. In Refs. [19,20] we describe the electron

weight [ELW, a statistic computed from pulse heights in the hodoscopes and Cerenkov counter and characteristics of the CCAL clusters, developed to discriminate among single electrons (positrons), electron-positron pairs from γ conversion, and hadrons]. We require that the product of the ELW for the two tracks constituting an event be less than 10^{-4}.

The event totals, for the selection described above, are tabulated in Tables I and II.

C. $J/\psi\gamma$ event selection

For this analysis we consider $a1$ triggers where the invariant mass of any two CCAL clusters is $\geqslant 2.2$ GeV, and each is within the angular region $15° < \theta < 60°$. We require that both clusters be associated with hodoscope hits and at least one be associated with a Cerenkov signal. Any number of additional on-time CCAL clusters within the angular region $12° < \theta < 68°$ are allowed in order to include radiative decays of the J/ψ and/or electron bremsstrahlung. We attempt 5 constraint kinematical fits to the hypothesis $\bar{p}p \to J/\psi\gamma \to e^+e^-\gamma$ and choose the best fit if its confidence level is $\geqslant 0.1\%$. We require the product of the ELW for the charged tracks to be greater than 1.5. The selected events are tabulated in Tables I and II.

D. Background determination

Accurate determination of the background is essential for estimation of the resonance signal. For the $J/\psi\gamma$ final state, the signal to background ratio is large and the background is smoothly varying [21]. However for the $\gamma\gamma$ final state, the signal to background ratio is less than 1. Since the background is derived from the strongly energy- and angle-dependent $\pi^0\pi^0$ and $\pi^0\gamma$ reactions, the assumption of a smooth energy dependence over a large energy interval may give misleading results, as illustrated below.

For the χ_{c2}, the resonance is very narrow and we have abundant background data at nearby points. We obtain the background cross section by fitting the data away from the resonance (given in Table I). Taking $\alpha = 0.45$, the background is parametrized as

$$\sigma_{bkgd}(s) = A\left(\frac{s_0}{s}\right)^{B/2} \tag{1}$$

where $\sqrt{s_0} = 3556.2$ MeV is the nominal χ_{c2} mass so that A is the background cross section at the resonance peak. A, B, and cov(A,B) are determined from the fit ($\chi^2[df] = 41.2[39]$) to be 22.3 ± 0.8 pb, 4.5 ± 2.5, and -0.51 pb respectively. The data and fit are shown in Fig. 4. The differential cross section for the χ_{c2} region is shown in Fig. 3, where we also show background data taken at 3526 MeV during the search for the h_c. The background angular distribution is required for determination of the angular acceptance cut.

The χ_{c0} is much broader, the nearest background points on either side are approximately 100 MeV away, and the cross sections have relatively large errors. The background is principally $\pi^0\gamma$ and $\pi^0\pi^0$events where one or two photons

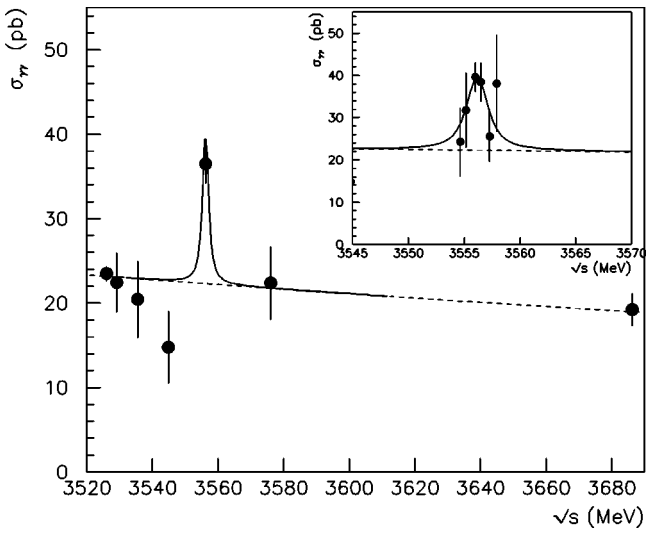

FIG. 4. $\gamma\gamma$ data used for the χ_{c2} analysis, with the acceptance cut $\cos\theta^* \leqslant 0.45$. The dashed curve is the fit to a background parametrized by Eq. (1). The solid curve is the result of our determination of signal and background, in which the resonance mass and width are fixed to 3556.2 MeV and 2.0 MeV respectively. The bin width for the main plot is 5.0 MeV; that for the inset is 0.75 MeV.

are undetected; for these reactions the angular distributions change rapidly in the vicinity of the χ_{c0} [22]. In order to accurately determine the χ_{c0} background, we use the method of feeddown described in Refs. [17] and [23]. The $\pi^0\pi^0$ and $\pi^0\gamma$ cross sections are determined from the data. A fast calorimeter simulation [22] is used to estimate the number of events from the $\pi^0\pi^0$ and $\pi^0\gamma$ channels contributing to the $\gamma\gamma$ background, where the differential cross sections for those reactions are determined from the data. The statistical errors are those of the measured $\pi^0\pi^0$ and $\pi^0\gamma$ cross sections. We estimate systematic errors, which we add in quadrature, to be approximately 6% by examining the degree to which varying the cuts used to select the $\pi^0\pi^0$ and $\pi^0\gamma$ events changes the observed cross sections and the degree of anisotropy (due to the loss of asymmetrically decaying π^0's) in the π^0 decay distribution. We have studied the performance of the feeddown method and have demonstrated that it reproduces the background cross sections at high statistics data points throughout the range of the experiment. In Fig. 5, along with the data and feeddown backgrounds used in the analysis, we show additional measured and feeddown cross sections between 3215.7 MeV and 3494.4 MeV. In Table II, we give the recorded and feeddown $\gamma\gamma$ event totals for data points at 3525.8 MeV and 3686.1 MeV. We have also found that subtraction of the feeddown background restores the forward-backward symmetry, required by charge conjugation invariance, of the differential cross section for the reaction $\bar{p}p \to \pi^0\gamma$ [22]. We proceed by subtracting the feeddown cross section from the observed $\gamma\gamma$ cross section for each energy in the resonance region, giving the excitation curve shown in Fig. 6. We obtain the differential cross section of the background, shown in Fig. 3 along with that of the signal, from the feeddown calculation. The background angular distribution is used for determination of the angular acceptance cut.

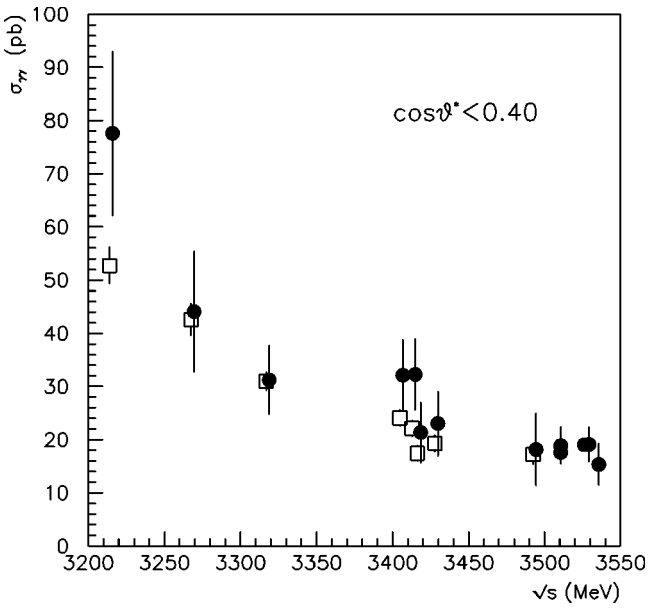

FIG. 5. The data (circles) and feeddown calculation (squares) used for the χ_{c0} analysis, with the acceptance cut $\cos\theta^* \leqslant 0.40$. The feeddown points are offset -2 MeV in $\sqrt{s}$ for clarity.

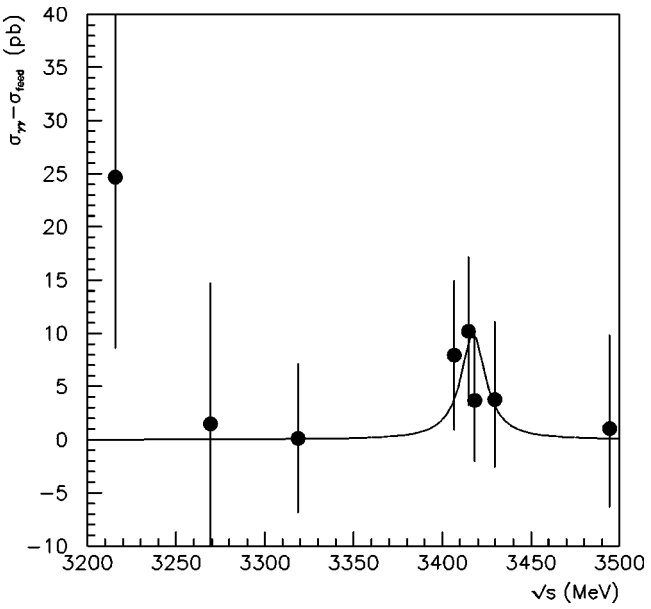

FIG. 6. The data shown are the observed $\gamma\gamma$ cross sections less the simulated feeddown cross sections in the vicinity of the χ_{c0}, for the acceptance cut $\cos\theta^* \leqslant 0.40$. The curve is our determination of the signal and is Breit-Wigner with resonance mass and width of 3417.4 MeV and 16.6 MeV respectively.

Together, the data and feeddown calculation do not allow for any contribution to the background from the continuum process $\bar{p}p \to \gamma\gamma$. The inverse reaction has been observed by VENUS [24] in the interval 2.2 GeV$\leqslant\sqrt{s}\leqslant$3.3 GeV but with very low statistics (1 event/point) at 3.05 and 3.3 GeV. A rough extrapolation of the VENUS result suggests a continuum $\gamma\gamma$ cross section of several pb at most at the χ_{c0} energy. This uncertainty is comparable to the uncertainty in the feeddown cross section.

E. Efficiency and acceptance determination

1. $\gamma\gamma$ efficiency and acceptance

The overall efficiency for the $\gamma\gamma$ channel is

$$\epsilon_{\gamma\gamma} \equiv \epsilon_{calo}(1-P_{cont})(1-P_{conv})^2. \qquad (2)$$

ϵ_{calo} is the efficiency for capturing $\gamma\gamma$ events and includes the triggering and analysis efficiencies, which cannot be separated because they are determined by the same counters. ϵ_{calo} is computed by simulation and elements of this efficiency are checked using J/ψ data. Since the trigger requires CCAL signals for both photons, an event can be missed if one or both photons deposit substantial energy into a dead CCAL channel. The effects of dead channels are included in the simulation [22] used to obtain ϵ_{calo}, which is calculated as a function of $\sqrt{s}$ and $\cos\theta^*$. Here ϵ_{calo} is approximately 0.9 and is nearly independent of $\sqrt{s}$ and $\cos\theta^*$, except for a localized dip of about 10% in the $\cos\theta^*$ dependence. This is due to three dead CCAL counters in two adjacent rings, and the dip appears at different $\cos\theta^*$ for different beam momenta.

We study ϵ_{calo} at the J/ψ energy, using a sample of more than 17 000$J/\psi \to {}^+e^-$ events, which have the same pattern of CCAL energy deposition as $\gamma\gamma$ events. These are selected with weak CCAL criteria: exactly two CCAL clusters with energies above 25 MeV with centers in rings 2–18, the two cluster invariant mass $\geqslant$2.0 GeV and the product of the *ELW* for the charged tracks >10, thus omitting the *PBG*1 and *ETOT* requirements. Based on the results of a dedicated run in which J/ψ events are collected with a trigger that does not require CCAL signals, we determine that this e^+e^- selection has unit efficiency. Application of the $\gamma\gamma$ event selection to the CCAL data for this event sample yields an ϵ_{calo} consistent with a simulation performed at the J/ψ energy. Using the same J/ψ data set, we examine the response of the standard trigger, finding that the *PBG*1 bit is off for $<0.01\%$ of the events and the *ETOT* bit is off for $<0.2\%$ of the events. All of the J/ψ events survive a $\geqslant$2.2 GeV two-cluster invariant-mass cut.

P_{cont} is the probability that an additional event contaminates a good event, causing it to be rejected. If such an event occurs within $\sim$10 ns of a $\gamma\gamma$ event, its signals are recorded as elements of the $\gamma\gamma$ event, which is now rejected by either the trigger or the analysis if the combined event has any of the properties described above; namely, the charged veto is on, the event has one or more in-time clusters in CCAL, or an undetermined cluster in the CCAL forms an invariant mass within the window [100,170] MeV when combined with an in-time cluster. We determine P_{cont} using events from the random gate trigger, which for each data point are superimposed on the neutral triggers. The factor $(1-P_{cont})$ varies from $\sim$0.93 at $\mathcal{L}\sim 0.7\times 10^{31}$ to $\sim$0.78 at $\mathcal{L}\sim 3.0\times 10^{31}$ [22], the luminosity range for these data.

P_{conv} is the probability that either photon converts into a e^+e^- pair before reaching the first detector element (H1). For our detector, averaged over the angular distribution of

the $\gamma\gamma$ events, $P_{conv}=0.011\pm0.001$.

There is a small dead time contribution ($<2\%$) to the inefficiency due to triggers employed for efficiency studies. The overall efficiency for each data point is given in Tables I and II.

The geometrical acceptance $a_{\gamma\gamma}$ is computed to be 0.56 ± 0.02 for the χ_{c2}, where the error comes from the uncertainty in the decay angular distribution, assumed to be $(1-\cos^4\theta^*)$. $a_{\gamma\gamma}$ is 0.40 for the χ_{c0}.

2. J/ψ γ efficiency and acceptance

The overall efficiency for the J/ψ γ channel is written as

$$\epsilon_{J/\psi\gamma}\equiv\epsilon_{trig}\epsilon_{anal}. \tag{3}$$

The trigger efficiency is determined to be $\epsilon_{trig}=0.90\pm0.01$ using the dedicated J/ψ run with relaxed trigger conditions referred to above. We obtain the analysis efficiency ϵ_{anal} from a clean sample of χ_{c1} and χ_{c2}. It is the product of the fit efficiency and the efficiency of the electron weight selection. The fit probability and the ELW product are nearly independent for this data set and we evaluate the efficiency of each selection by making a tight cut on the variable corresponding to the other, giving $\epsilon_{anal}=0.83\pm0.02$.

The geometrical acceptance $a_{J/\psi\gamma}$ is based on the requirement that electrons be in the Cerenkov fiducial region $15°<\theta<60°$ and photons be in the CCAL fiducial region $12°<\theta<68°$. It is determined by simulation to be 0.44 ± 0.01 for the χ_{c2} and 0.35 ± 0.01 for the χ_{c0}.

IV. RESULTS

A. Branching ratio determination

We determine the χ_{c2} and χ_{c0} branching ratios to $\gamma\gamma$ by measuring the ratios of rates to the final states: $\gamma\gamma$ and $J/\psi\gamma$. The data sets used in the analysis are given in Tables I and II, where the data points used for the ratio determination are marked with an asterisk and the remaining points are used for background determinations. We define R, the ratio of the two branching ratios, as follows:

$$R\equiv\frac{B(\chi\to\gamma\gamma)}{B(\chi\to J/\psi\gamma\to e^+e^-\gamma)}=\frac{\sigma(\bar{p}p\to\chi\to\gamma\gamma)}{\sigma(\bar{p}p\to\chi\to J/\psi\gamma\to e^+e^-\gamma)}. \tag{4}$$

Written in terms of numbers of events, the ratio for a single data point is

$$R_i=\frac{\frac{1}{a_{\gamma\gamma}\epsilon_{\gamma\gamma i}}[N_{\gamma\gamma i}-N_{bkgd,\gamma\gamma i}]}{\frac{1}{a_{J/\psi\gamma}\epsilon_{J/\psi\gamma}}[N_{J/\psi\gamma i}-N_{bkgd,J/\psi\gamma i}]}. \tag{5}$$

N is the number of events, a is the geometrical acceptance, and ϵ is the combined analysis and trigger efficiency. $N_{bkgd,\gamma\gamma i}$ for the χ_{c0} are the feeddown results. Since the χ states are narrow compared to the scale of variation for the background, we take the remaining background cross sections to be independent of $\sqrt{s}$. Here N_{bkgd}, except for the $\gamma\gamma$ background for the χ_{c0}, are then given by

TABLE III. Parameters used to calculate R for the χ_{c2}.

$\sigma_{bkgd,J/\psi\gamma}$	6.09 ± 0.86 pb
$\sigma_{bkgd,\gamma\gamma}$	39.6 ± 1.1 pb
$a_{J/\psi\gamma}$	0.44 ± 0.01
$\epsilon_{J/\psi\gamma}$	0.75 ± 0.01
$a_{\gamma\gamma}$	0.56 ± 0.02

$$N_{bkgd,\gamma\gamma}=\epsilon_{\gamma\gamma}a_{\gamma\gamma}\sigma_{bkgd,\gamma\gamma}\int\mathcal{L}dt \tag{6}$$

$$N_{bkgd,J/\psi\gamma}=\epsilon_{J/\psi\gamma}a_{J/\psi\gamma}\sigma_{bkgd,J/\psi\gamma}\int\mathcal{L}dt. \tag{7}$$

The efficiency $\epsilon_{\gamma\gamma}$ depends upon the instantaneous luminosity, while $\epsilon_{J/\psi\gamma}$ varies less than 1% with luminosity for the data points considered and is assumed constant when calculating R. The values of σ_{bkgd}, a, and $\epsilon_{J/\psi\gamma}$ are given in Tables III and IV.

The individual R_i may be useful for studying possible systematic effects within the rather large statistical errors. Figure 7 shows R_i as a function of mean instantaneous luminosity and of center of mass energy for the data at the χ_{c2} resonance. A variation with luminosity may be caused by an error in the efficiency calculation $\epsilon_{\gamma\gamma}$, while a variation with center-of-mass energy may be caused by an error in the background determination. Figure 8 contains the corresponding plots for the χ_{c0} resonance. No significant variation is seen for either state.

We compute the overall R as follows:

$$R=\frac{\frac{1}{a_{\gamma\gamma}}\left[\sum_i\frac{1}{\epsilon_{\gamma\gamma i}}(N_{\gamma\gamma i}-N_{bkgd,\gamma\gamma i})\right]}{\frac{1}{\epsilon_{J/\psi\gamma}a_{J/\psi\gamma}}\left[\sum_i(N_{J/\psi\gamma i}-N_{bkgd,J/\psi\gamma i})\right]}. \tag{8}$$

For the χ_{c2}, taking the $\chi_{c2}\to J/\psi\gamma\to e^+e^-\gamma$ branching ratio of $(0.81\pm0.07)\times10^{-2}$ and χ_{c2} width of $\Gamma=2.00\pm0.18$ MeV from Ref. [25], we find

TABLE IV. Parameters used to calculate R for the χ_{c0}.

$\sigma_{bkgd,J/\psi\gamma}$	8.01 ± 1.05 pb
$a_{J/\psi\gamma}$	0.35 ± 0.01
$\epsilon_{J/\psi\gamma}$	0.75 ± 0.01
$a_{\gamma\gamma}$	0.40

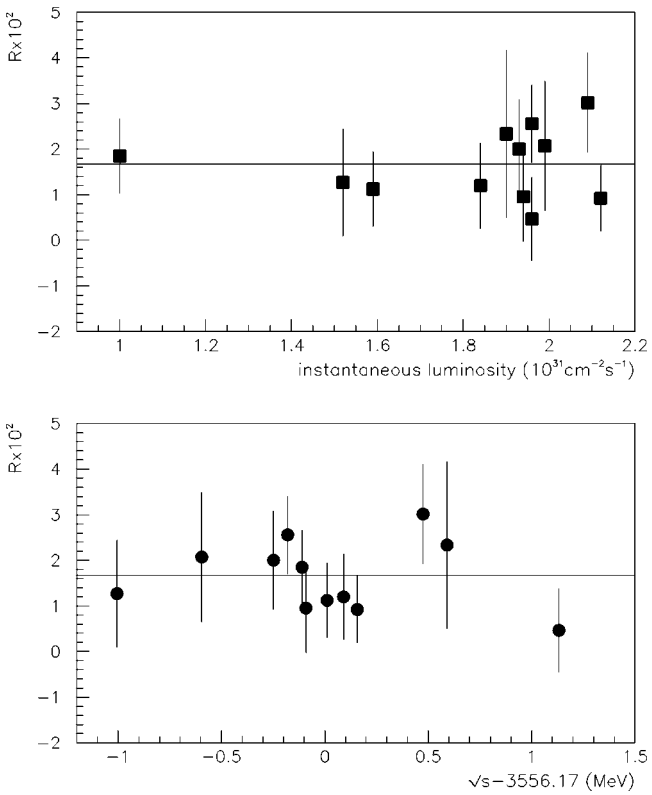

FIG. 7. The ratio R for the χ_{c2} data plotted against mean instantaneous luminosity (above) and $\sqrt{s}$ (below). The line gives the overall R.

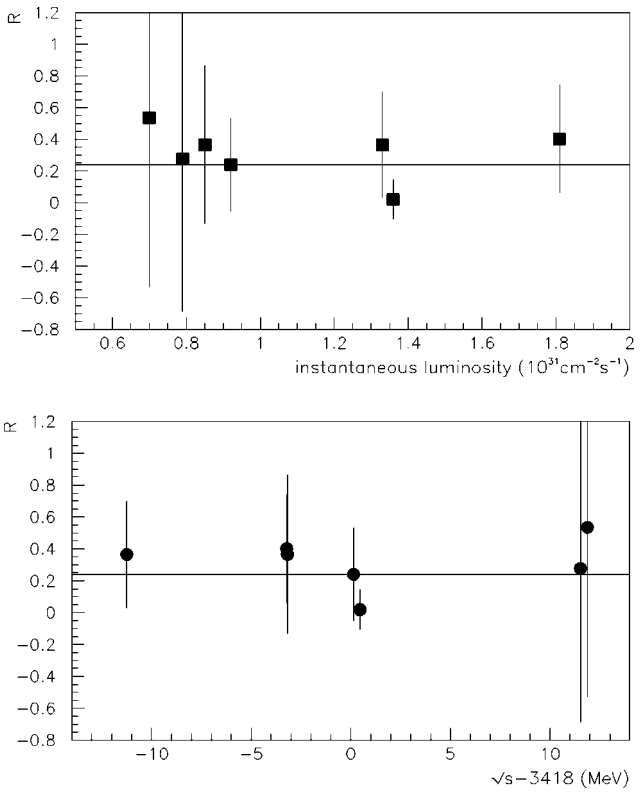

FIG. 8. The ratio R for the χ_{c0} data plotted against mean instantaneous luminosity (above) and $\sqrt{s}$ (below). The line gives the overall R.

$$R = (1.67 \pm 0.30) \times 10^{-2} \tag{9}$$

$$B(\chi_{c2} \to \gamma\gamma) = (1.35 \pm 0.25 \pm 0.12) \times 10^{-4} \tag{10}$$

$$\Gamma(\chi_{c2} \to \gamma\gamma) = 270 \pm 49 \pm 33 \ \text{eV}. \tag{11}$$

The error on R is dominated by the low statistics of the $\gamma\gamma$ channel. The uncertainties in $\epsilon_{\gamma\gamma}$, $a_{\gamma\gamma}$, $\epsilon_{J/\psi\gamma}$, $a_{J/\psi\gamma}$, $\sigma_{bkgd,\gamma\gamma}$, and $\sigma_{bkgd,J/\psi\gamma}$ contribute approximately 5% in all to the error. The first errors quoted include these contributions and counting statistics. The second error for $B_{\gamma\gamma}$ comes from the uncertainty in $B_{J/\psi\gamma}$ and that for $\Gamma_{\gamma\gamma}$ contains, in addition, a contribution from Γ. In Fig. 9 we compare our value for $\Gamma(\chi_{c2} \to \gamma\gamma)$ with those of the experiments listed in Table V and the theoretical predictions given in Table VI.

For the χ_{c0}, taking the $\chi_{c0} \to J/\psi\gamma \to e^+e^-\gamma$ branching ratio to be $(3.97 \pm 1.15) \times 10^{-4}$ from Ref. [25] and the χ_{c0} width to be $\Gamma = 16.6 \pm {}^{5.2}_{3.7}$ MeV from Ref. [21], we find

$$R = 0.244 \pm 0.125 \tag{12}$$

$$B(\chi_{c0} \to \gamma\gamma) = (0.97 \pm 0.50 \pm 0.28) \times 10^{-4} \tag{13}$$

$$\Gamma(\chi_{c0} \to \gamma\gamma) = 1.61 \pm 0.83 \pm 0.65 \ \text{keV}. \tag{14}$$

The first errors include counting statistics and errors from efficiencies, acceptances and backgrounds and the second come from uncertainties in the χ_{c0} branching ratio to $J/\psi\gamma$ and width. This result can also be expressed as the upper limit

$$B(\chi_{c0} \to \gamma\gamma) \leqslant 2.09 \times 10^{-4} \ \ (95\%\ \text{C.L.}), \tag{15}$$

$$\Gamma(\chi_{c0} \to \gamma\gamma) \leqslant 3.47 \ \ \text{keV} \ \ (95\%\ \text{C.L.}). \tag{16}$$

In Fig. 10 we compare our value for $\Gamma(\chi_{c0} \to \gamma\gamma)$ with those of the experiments listed in Table V and the theoretical predictions given in Table VI.

An alternative analysis [26] which does not use the feed-down technique determines the background from data

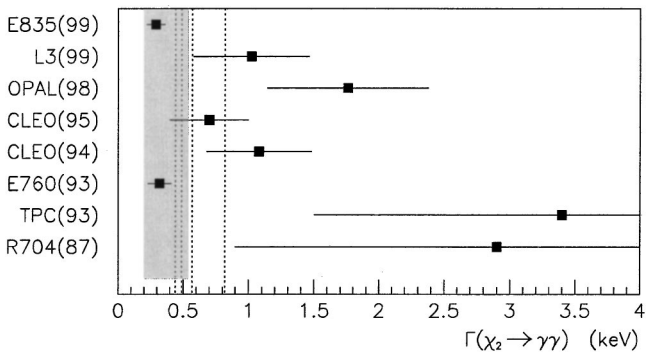

FIG. 9. Measurements of $\Gamma(\chi_{c2} \to \gamma\gamma)$. The shaded area represents the PDG 68.27% confidence interval and the dashed lines the theoretical predictions given in Table VI.

TABLE V. Prior experiments reporting $\gamma\gamma$ decay widths of χ_{c2} and χ_{c0} with their results in keV.

CBALL(85) [28]	$\psi' \to \chi_{c0}\gamma, \chi_{c0} \to \gamma\gamma$	4.0 ± 2.8
R704(87) [29]	$\bar{p}p \to \chi_{c2} \to \gamma\gamma$	2.9 ± 2.1
CLEO(90) [30]	$\gamma\gamma \to \chi_{c0} \to$ hadrons	<6.2(95%)
TPC(93) [31]	$\gamma\gamma \to \chi_{c2} \to J/\psi\gamma, J/\psi \to l^+l^-$	3.4 ± 1.9
E760(93) [27]	$\bar{p}p \to \chi_{c2} \to \gamma\gamma$	0.32 ± 0.09
CLEO(94) [32]	$\gamma\gamma \to \chi_{c2} \to J/\psi\gamma, J/\psi \to l^+l^-$	1.08 ± 0.4
CLEO(95) [33]	$\gamma\gamma \to \chi_{c2} \to$ hadrons	0.7 ± 0.3
	$\gamma\gamma \to \chi_{c0} \to$ hadrons	1.7 ± 0.8
OPAL(98) [34]	$\gamma\gamma \to \chi_{c2} \to J/\psi\gamma, J/\psi \to l^+l^-$	1.76 ± 0.62
L3(99) [35]	$\gamma\gamma \to \chi_{c2} \to J/\psi\gamma, J/\psi \to l^+l^-$	1.02 ± 0.44

points outside the resonance region. This approach assumes a smooth background (in the region from 3200 to 3700 MeV) which may not be the case since the $\pi^0\pi^0$ channel of the resonance and continuum may interfere. This analysis uses $B(\chi_{c0} \to \bar{p}p)$ and the total width from Ref. [21] and gives

$$B(\chi_{c0} \to \gamma\gamma) = (0.26 \pm 0.38 \pm 0.10) \times 10^{-4} \tag{17}$$

$$\Gamma(\chi_{c0} \to \gamma\gamma) = 0.43 \pm 0.63 \pm 0.16 \text{ keV}, \tag{18}$$

which correspond to the upper limits

$$B(\chi_{c0} \to \gamma\gamma) \leqslant 1.03 \times 10^{-4} \quad (95\%\ \text{C.L.}) \tag{19}$$

$$\Gamma(\chi_{c0} \to \gamma\gamma) \leqslant 1.70 \text{ keV} \quad (95\%\ \text{C.L.}). \tag{20}$$

B. Sensitivity of results to acceptance cut

In order to investigate the sensitivity of the results to the angular cut, we perform the analyses for the χ_{c0} and χ_{c2} resonances using acceptance cuts $\cos\theta^* < \alpha$ both larger and smaller than the optimal values found using the procedure of the Appendix. For the χ_{c2}, the branching ratio taking $\alpha = 0.40(0.50)$ is $(1.46 \pm 0.26 \pm 0.13) \times 10^{-4}$[$(1.45 \pm 0.25 \pm 0.13) \times 10^{-4}$]. The result for the optimal $\alpha = 0.45$ of $(1.35 \pm 0.25 \pm 0.12) \times 10^{-4}$ is a local minimum. For the χ_{c0}, taking $\alpha = 0.35(0.45)$ yields a branching ratio of $(0.91 \pm 0.46 \pm 0.26) \times 10^{-4}$[$(1.66 \pm 0.62 \pm 0.48) \times 10^{-4}$] compared to that for the optimal $\alpha = 0.40$ of $(0.97 \pm 0.50 \pm 0.28) \times 10^{-4}$. While the result is stable for $\alpha \leqslant 0.40$, it increases abruptly for $\alpha = 0.45$ as a consequence of the single high data point at $\cos\theta^* = 0.425$ shown in Fig. 3.

TABLE VI. Some theoretical predictions for two photon decays of χ_{c0} and χ_{c2}. The predictions of Barnes are for $m_c = 1.6(1.4)$ GeV.

	$\Gamma(\chi c0 \to \gamma\gamma)$ (keV)	$\Gamma(\chi c2 \to \gamma\gamma)$ (keV)
Huang and Chao *et al.* [2]	3.72 ± 1.11	0.49 ± 0.15
Gupta *et al.* [3]	6.38	0.57
Münz [4]	1.39 ± 0.16	0.44 ± 0.14
Bodwin *et al.* [5]	$11.3 \pm {}^{4.7}_{4.0}$	0.82 ± 0.23
Barnes [6]	1.56(0.96)	0.56(0.34)

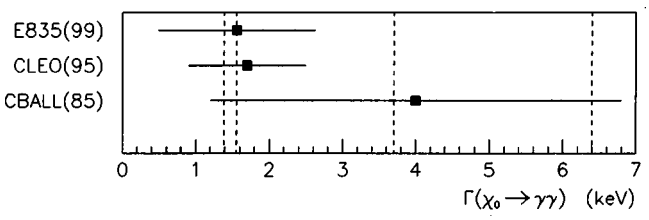

FIG. 10. Measurements of $\Gamma(\chi_{c0} \to \gamma\gamma)$. The dashed lines are the theoretical predictions given in Table VI.

C. Calculation of $\alpha_s(m_c)$

Our data for $\Gamma(\chi_{c2} \to \gamma\gamma)$ allow estimation of $\alpha_s(m_c)$, the strong coupling constant. Reference [7] gives PQCD formulas with first order radiative corrections for the electromagnetic and gluonic decay widths of charmonium states. The ratio of partial widths depends only on $\alpha_s(m_c)$. We have

$$\frac{\Gamma(\chi_{c2} \to \gamma\gamma)}{\Gamma(\chi_{c2} \to gg)} = \frac{8\alpha^2}{9\alpha_s^2} \frac{\left[1 - \frac{16}{3\pi}\alpha_s\right]}{\left[1 - \frac{2.2}{\pi}\alpha_s\right]} \Rightarrow \alpha_s(m_c) = 0.38 \pm 0.02 \tag{21}$$

where we take

$$\frac{\Gamma(\chi_{c2} \to \gamma\gamma)}{\Gamma(\chi_{c2} \to gg)} \approx \frac{B(\chi_{c2} \to \gamma\gamma)}{1 - B(\chi_{c2} \to J/\psi\gamma)}.$$

This result is compatible with that of E760, $\alpha_s = 0.36 \pm 0.04$ [27], and with the best fit to the energy dependence of α_s given by Ref. [25]. The latter value is sensitive to m_c, the charm quark mass, given by Particle Data Group (PDG) as 1.3 ± 0.3 GeV. For $m_c = 1.3$ GeV, the fit yields 0.36 ± 0.02.

Rather than use our poor determination of $B(\chi_{c0} \to \gamma\gamma)$ to estimate α_s, we compare the prediction of PQCD for the ratio of χ_{c0} branching ratios with our measurement, using $\alpha_s = 0.36 \pm 0.02$:

$$\frac{\Gamma(\chi_{c0} \to \gamma\gamma)}{\Gamma(\chi_{c0} \to gg)} = \frac{8\alpha^2}{9\alpha_s^2} \frac{\left[1 + \frac{0.2}{\pi}\alpha_s\right]}{\left[1 + \frac{9.5}{\pi}\alpha_s\right]} \Rightarrow B(\chi_{c0} \to \gamma\gamma) = (1.75 \pm {}^{0.23}_{0.19}) \times 10^{-4}. \tag{22}$$

The predicted value is larger than but statistically compatible with our measurement $B(\chi_{c0} \to \gamma\gamma) = (0.97 \pm 0.50 \pm 0.28) \times 10^{-4}$.

V. CONCLUSIONS

We have studied the $\gamma\gamma$ decays of the χ_{c2} and χ_{c0} by observing these resonances formed in $\bar{p}p$ annihilation, in contrast to other recent determinations which observe $\gamma\gamma$ interactions resulting from e^+e^- scattering. Our result for the χ_{c2} branching ratio is in good agreement with that of our previous experiment E760, but is smaller than that reported by other experiments. Our result for the χ_{c0} branching ratio is compatible with those reported by CLEO and Crystal Ball and is also compatible with no signal. The theoretical estimates given in Table VI vary widely; the smaller of the predictions are approximately consistent with our results.

ACKNOWLEDGMENTS

The authors wish to gratefully acknowledge the technical support provided by Fermilab, in particular by the Antiproton Source Department of the Beams Division and the Online Support Department of the Computing Division. They also wish to thank the staff, engineers, and technicians at our respective institutions for their help and cooperation. This research was supported by the U.S. Department of Energy and the Italian Istituto Nazionale di Fisica Nucleare.

APPENDIX: OPTIMIZATION OF THE $\gamma\gamma$ ANGULAR ACCEPTANCE

The angular distribution of $\chi_{c0}\to\gamma\gamma$ decay is isotropic and that of $\chi_{c2}\to\gamma\gamma$ is not strongly peaked. In contrast, the background reactions, $\bar{p}p\to\pi^0\gamma$ and $\bar{p}p\to\pi^0\pi^0$ are strongly forward peaked as discussed above.

The uncertainty in the resonance cross section is maximized by choosing a maximum $\cos\theta^*$, where θ^* is the center of mass angle. We determine the optimal cutoff in $\cos\theta^*$, designated here as α, using the measured angular and energy dependence of the background cross section. We take the signal angular distributions to be uniform for the χ_{c0} and $(1-\cos^4\theta^*)$ [27] for the χ_{c2}, the latter based on the PQCD expectation of a helicity 1 initial state and helicity 2 final state.

For a peak signal cross section σ_{peak}, the expected event total at each energy $\sqrt{s_i}$, for cutoff α, is given by

$$E(N_{\gamma\gamma i}(\alpha))=\mathcal{L}_i\epsilon_i[\sigma_{bkgd}(s_i,\alpha)+\sigma_{peak}a(\alpha)BW(s_i)] \tag{A1}$$

$$BW(s_i)\equiv\int f_i(s')\frac{\Gamma_R^2}{4(\sqrt{s'}-M_R)^2+\Gamma_R^2}ds' \tag{A2}$$

where $f_i(s)$ is the normalized beam energy distribution at energy $\sqrt{s_i}$ and

$$a(\alpha)\equiv\int_0^\alpha w(\cos\theta^*)d(\cos\theta^*) \tag{A3}$$

where $w(\cos\theta^*)$ is the angular distribution of the two photon decay.

We estimate σ_{peak} using linear regression, giving

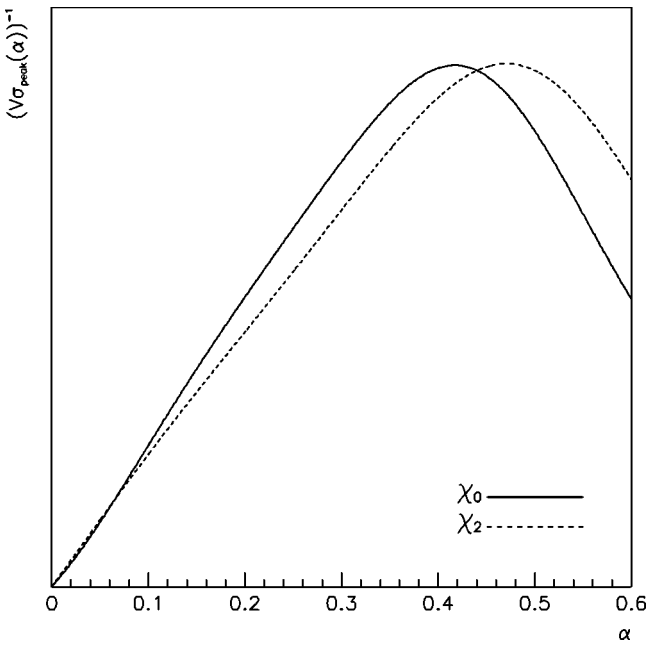

FIG. 11. $(V_{\sigma_{peak}(\alpha)})^{-1}$, in arbitrary units, as a function of the acceptance cut α for the χ_{c2} and χ_{c0} resonances. The two curves are not on the same scale.

$$\hat{\sigma}_{peak}=V_{\sigma_{peak}}(\alpha)\times\sum_i\frac{[N_{\gamma\gamma i}(\alpha)-\mathcal{L}_i\epsilon_i\sigma_{bkgd}(s_i,\alpha)]\mathcal{L}_i\epsilon_i a(\alpha)BW(s_i)}{V_i(\alpha)} \tag{A4}$$

$$V_{\sigma_{peak}}(\alpha)=\left(\sum_i\frac{[\mathcal{L}_i\epsilon_i a(\alpha)BW(s_i)]^2}{V_i(\alpha)}\right)^{-1} \tag{A5}$$

where $V_i(\alpha)$ is the variance for $N_{\gamma\gamma i}$, the number of events observed at energy $\sqrt{s_i}$. Here $\hat{\sigma}_{peak}$, the least squares estimate of σ_{peak}, is distributed approximately normally about the true value with variance $V_{\sigma_{peak}}(\alpha)$.

We seek an angular cutoff that optimizes our ability to detect a resonance signal. In this case, this procedure is equivalent to minimizing the uncertainty in the signal cross section. Under the hypothesis H0 $[\sigma_{peak}=0]$ that no resonance signal exists, $\hat{\sigma}_{peak}$ is distributed normally about zero and can be used as a statistic to test H0. For arbitrary significance, we can maximize the power of a test for H0 versus the alternate hypothesis H1 $[\sigma_{peak}>0]$ by choosing the parameter α to minimize $V_{\sigma_{peak}}(\alpha)$. Assuming Poisson statistics, thus taking

$$V_i(\alpha)=\mathcal{L}_i\epsilon_i[\sigma_{bkgd}(s_i,\alpha)+\sigma_{peak}a(\alpha)BW(s_i)], \tag{A6}$$

we have

$$V_{\sigma_{peak}}(\alpha)=\left(\sum_i\frac{\mathcal{L}_i\epsilon_i[a(\alpha)BW(s_i)]^2}{\sigma_{bkgd}(s_i,\alpha)+a(\alpha)\sigma_{peak}BW(s_i)}\right)^{-1}. \tag{A7}$$

We observe that for $\sigma_{bkgd}=0$, $V_{\sigma_{peak}}/\hat{\sigma}^2_{peak}=1/N$ where N is the total number of recorded events.

There is an optimal cutoff if $\sigma_{bkgd}(s,\alpha)$ increases faster than $\sim\alpha^2$. This is easily seen. The α dependence of a single term from Eq. (A7), for an isotropically decaying resonance $[a(\alpha)=\alpha]$, is $[\sigma_{bkgd}(\alpha)+\alpha\sigma_{peak}BW]/\alpha^2$ where we have dropped the argument s_i. The minimum V satisfies $\alpha d\sigma_{bkgd}(\alpha)/d\alpha-2\sigma_{bkgd}(\alpha)=\alpha\sigma_{peak}BW$. For simplicity, we consider a background cross section of the form $\sigma_{bkgd}=A\alpha^n$. For isotropic $(n=1)$ or linear $(n=2)$ background the minimum V is found for $\alpha=1$. For $n>2$, we have an optimal $\alpha<1$ which equals, for $n=3$, $\sqrt{\sigma_{peak}BW/A}$.

Using the $\mathcal{L}_i$ and ϵ_i given in Tables I and II, we obtain $[V_{\sigma_{peak}}(\alpha)]^{-1}$ for the χ_{c2} and χ_{c0} as a function of α as shown in Fig. 11. We take σ_{peak} for the χ_{c2} to be 43 pb based on current PDG values and σ_{peak} for the χ_{c0} to be 29 pb based on the approximate signal expected. We find that for the χ_{c2}, increasing σ_{peak} by a factor of 10 increases the optimal cutoff by 0.14. For the χ_{c0}, the optimum cutoff increases by 0.10 for a 10 times larger peak cross section. We choose $\alpha=0.45$ and $\alpha=0.40$ for the χ_{c2} and χ_{c0}, respectively.

[1] R. Barbieri *et al.*, Nucl. Phys. **B154**, 535 (1979).
[2] H.-W. Huang and K.-T. Chao, Phys. Rev. D **54**, 6850 (1996); **56**, 1821(E) (1997).
[3] S. N. Gupta, J. M. Johnson, and W. W. Repko, Phys. Rev. D **54**, 2075 (1996).
[4] C. R. Münz, Nucl. Phys. **A609**, 364 (1996).
[5] G. Bodwin, E. Braaten, and G. P. Lepage, Phys. Rev. D **51**, 1125 (1995).
[6] T. Barnes, in *Proceedings of the 9th International Workshop on Photon-Photon Collisions*, La Jolla, California, 1992, edited by H. Paar and D. Caldwell (World Scientific, Singapore, 1992), pp. 263–274.
[7] W. Kwong, P. B. Mackenzie, R. Rosenfeld, and J. L. Rosner, Phys. Rev. D **37**, 3210 (1988).
[8] M. Church and J. Marriner, Annu. Rev. Nucl. Part. Sci. **43**, 253 (1993).
[9] D. Allspach *et al.*, Nucl. Instrum. Methods Phys. Res. A **410**, 195 (1998).
[10] S. Bagnasco *et al.*, Nucl. Instrum. Methods Phys. Res. A **409**, 75 (1998).
[11] M. Ambrogiani *et al.*, Nucl. Instrum. Methods Phys. Res. A **419**, 632 (1998).
[12] S. Bagnasco *et al.*, Nucl. Instrum. Methods Phys. Res. A **424**, 304 (1999).
[13] L. Bartoszek *et al.*, Nucl. Instrum. Methods Phys. Res. A **301**, 47 (1991).
[14] S. Trokenheim *et al.*, Nucl. Instrum. Methods Phys. Res. A **355**, 308 (1995).
[15] G. Oleynik *et al.*, IEEE Trans. Nucl. Sci. **43**, 20 (1996).
[16] R. Ray *et al.*, Nucl. Instrum. Methods Phys. Res. A **307**, 254 (1991).
[17] T. Armstrong *et al.*, Phys. Rev. D **52**, 4839 (1995).
[18] O. Dahl, T. Day, and F. Solmitz, Technical Report No. P-126, University of California Lawrence Radiation Laboratory.
[19] M. Ambrogiani *et al.*, Phys. Rev. D **60**, 032002 (1999).
[20] G. Garzoglio *et al.* (unpublished).
[21] M. Ambrogiani *et al.*, Phys. Rev. Lett. **83**, 2902 (1999).
[22] M. Stancari, Ph.D. thesis, University of California, Irvine, 1999.
[23] T. Armstrong *et al.*, Phys. Rev. D **56**, 2509 (1997).
[24] H. Hamasaki *et al.*, Phys. Lett. B **407**, 185 (1997).
[25] Particle Data Group, C. Caso *et al.*, Eur. Phys. J. C **3**, 1 (1998).
[26] T. Pedlar, Ph.D. thesis, Northwestern University, 1999.
[27] T. Armstrong *et al.*, Phys. Rev. Lett. **70**, 2988 (1993).
[28] R. A. Lee, Ph.D. thesis, Stanford University, 1985, Report No. SLAC-0282.
[29] C. Baglin *et al.*, Phys. Lett. B **187**, 191 (1987).
[30] W. Y. Chen *et al.*, Phys. Lett. B **243**, 169 (1990).
[31] D. Bauer *et al.*, Phys. Lett. B **302**, 345 (1993).
[32] J. Dominick *et al.*, Phys. Rev. D **50**, 4265 (1994).
[33] V. Savinov and R. Fulton, in *Proceedings of the 10th International Workshop on Photon-Photon Collisions*, edited by D. Miller *et al.* (World Scientific, Singapore, 1995), p. 203; hep-ex/9507006.
[34] K. Ackerstaff *et al.*, Phys. Lett. B **439**, 197 (1998).
[35] M. Acciarri *et al.*, Phys. Lett. B **453**, 73 (1999).